

Structural origin of spectral broadening of 1.5- μm emission in Er^{3+} -doped tellurite glasses

A. Jha,* S. Shen, and M. Naftaly

Department of Materials, Clarendon Road, University of Leeds, Leeds LS2 9JT, United Kingdom

(Received 20 July 1999; revised manuscript received 13 January 2000)

The emission spectra and the lifetimes of the lasing transition ${}^4I_{13/2}$ - ${}^4I_{15/2}$ in Er^{3+} -doped TeO_2 - ZnO - Na_2O ternary glasses have been studied. The investigation includes two main studies: The first part discusses the Raman spectroscopic analysis of the host glass structure. In the second part, we explain the dependence of Er^{3+} -ion photoluminescence near 1500 nm on OH^- -ion concentration. The influence of the concentrations of Er_2O_3 and the glass structure modifiers (ZnO , Na_2O) on the lifetimes of ${}^4I_{13/2}$ level and line shape of the emission spectra has been analyzed. It was observed that the increasing concentrations of Er^{3+} ions resulted in spectral broadening as a consequence of Er^{3+} being distributed in the glass structure. The measured lifetimes of ${}^4I_{13/2}$ emission vary between 4.5 and 7.8 ms and strongly depend on OH^- ion concentrations. The structural origin of the spectral broadening of the Er emission line is particularly discussed by analyzing the spectral components in the tellurite, modified silicate, and fluoride glass hosts. The number of spectral components at room temperature in Er-doped TeO_2 , silicate, and fluoride glasses are compared, and the dependence of line strengths and site-to-site variation of the rare-earth ions on the structure of each glass is also explained. The unusually large broadening of the OH^- band in the TeO_2 family of glasses is analyzed in the context of the tellurite glass structure.

I. INTRODUCTION

A rare-earth ion, for example, Er^{3+} doped in a glass host, when excited using a pump photon usually exhibits an inhomogeneously broadened emission line for a transition between the levels **a** and **b**. The amplifier channel gain is defined by the homogeneous spectral width, $\Delta\nu_{ab}$ of a lasing transition, which is dependent on the characteristics of the line-shape broadening. The spectral width $\Delta\nu_{ab}$ can be expressed as

$$\Delta\nu_{ab} = A_a + A_b + \frac{2}{T_{2(ab)}}, \quad (1)$$

where $A_{a,b}$ is the decay rates of the **a** and **b** levels, and $T_{2(ab)}$ is an effective relaxation rate associated with phonon broadening, which is also known as the dephasing time.¹ In a homogeneously broadened spectrum, due to the uniformity of the field around the rare-earth ions, a single frequency pump will interact with all the dopant ions with equal probability. The pump, therefore, produces a gain spectrum in which any signal wavelength can saturate the entire gain band. The uniformity of field around the rare-earth ions in a glass host will also enable signals at different wavelengths to interact with each other, which may be advantageous in a high-power laser and amplifiers. However, this feature will prove detrimental in a wavelength-division-multiplexing (WDM) system in which the power amplifiers may suffer from cross-saturation and cross-talk. On the other hand, the variations in the nearest-neighbor environment, local site symmetry, and ligand field strengths produce an inhomogeneously broadened spectrum. As a result of the site-to-site variations, there occurs a difference between the nonradiative and radiative rates, and individual sections of a gain spectrum respond independently, should these differences become large. In a WDM system, the cross-channel interaction

must be minimized, but not at the expense of a large variation in the power out of each channel. Gain excursion must be minimized. The design of a rare earth (RE)-doped glass that yields an inhomogeneously broadened spectrum with uniform output power for each channel will prove beneficial for WDM applications.

The low-loss window at 1.5 μm in the installed silica glass optical fiber networks is undergoing a major upgrading for a WDM operation. For an efficient WDM operation, the Er^{3+} -doped amplifiers with broadband and flat gain characteristics are required to compensate and maintain the gain at each channel, so that the gain excursion over the whole spectral width can be minimized. It is, therefore, essential that the dependence of the emission oscillator strength of a transition **a-b**, f_{ab} on host glass is understood for designing a broadband amplifier. The emission oscillator strength f_{ab} is dependent on local field correction, $(E_{\text{loc}}/E)^2 = \chi^2$, which is a host-dependent property. χ may be either due to electric dipole or magnetic dipole; in each case it is proportional to the square of the refractive index, n i.e., n^2 . By including the emission cross section (σ_{ab}) and local-field correction (χ), f_{ab} for a given transition **a-b** is proportional to the spectral integral of the cross section, which can be expressed by Eq. (2).^{2(a)} In Eq. (2), the summation sign defines all the sublevel transitions, of which the transition between the levels **a** and **b** is an example:

$$f_{ab} = \frac{Z_0 \cdot n}{\chi} \sum_{i=1}^{i=j} \Delta\nu_{ab} \sigma_{(ab)}^{\text{peak}}. \quad (2)$$

Z_0 is a constant in Eq. (2). Upon rearranging Eq. (2) yields that the line broadening ($\Delta\nu_{\text{eff}}$) is dependent upon two main factors: the local field effect determined by the ion-host interaction and the emission cross section. The ion-host interaction also determines the extent of Stark splitting. The

TABLE I. The identification of Raman peaks and their relative intensities determined from Gaussian peak fit program. The assignment of vibrational modes in TeO₂ glasses are based on the results reported in Refs. 19–22.

Glass composition (mol %)	Urbach edge (E_0), (eV)	Raman peak (ν_R) cm ⁻¹ and relative peak intensity (%)				
		Peak A	Peak B	Peak C	Peak D	Peak E
80 TeO ₂ , 10 ZnO, 10 Na ₂ O (RR2)	5.44	440 (48%)	591 (19%)	663 (91%)	730 (42%)	778 (49%)
90 TeO ₂ , 10 ZnO (RR14)	5.08	420 (53%)	601 (19%)	656 (77%)	717 (30%)	768 (38%)
60 TeO ₂ , 10 ZnO, 20 Na ₂ O (RR15)	6.25	450 (17%)	583 (9%)	681 (51%)	765 (64%)	793 (31%)
α -TeO ₂		450	611	659	716	773

emission cross-section together with the lifetime (τ) of metastable level **b** determines the gain (G) of an amplifier, i.e., $G \propto (\sigma\tau)$.

Two main methods have already been adopted for broadening and flattening the gain curve in Er-doped silica devices. The first approach is based on modifying the structure of host glass by incorporating Al₂O₃ and P₂O₅ codoping of silica glass (known as Al/P silica),³ which is known to disperse Er³⁺ ions in the silica glass matrix and thereby provide multiple sites. The modification of glass structure with Al₂O₃P₂O₅ addition leads to an increase in the value of the full width at half maximum (FWHM) from 8 nm in pure silica to 44 nm in Al/P silica.^{2(b)} A significant spectral flattening has been also achieved via filtering reported by Georges.⁴ From Eq. (2) the emission cross section increases with the increasing refractive index of the host glass. The value of the FWHM is 65 nm for the 1500 nm transition in Er³⁺-doped fluorozirconate family of glasses.^{5,6} Consequently Er³⁺-doped fluorozirconate glass fiber amplifiers have been considered as an alternative to Al/P silica-based devices. Although the emission and the gain curves are much broader in Er-doped zirconium-barium-lanthanum-aluminium-sodium-fluoride (ZBLAN) glass, it suffers from three main disadvantages. The first disadvantage is related with the low phonon energy of ZBLAN host (580 cm⁻¹), which makes the device unsuitable for pumping at 980 nm due to an enhanced excited state absorption at pump wavelength.⁷ As a result, the device is only pumped at 1480 nm. The second major problem is that the glass cannot be heavily doped with Er³⁺, as the concentration quenching starts dominating above 1000 ppm concentration level.^{8–11} The third problem is the comparatively poor stability and durability of ZBLAN fibers. It is much weaker than Al/P silica. The unsuitability of Er³⁺-doped ZBLAN and limitation of Al/P silica led to a search for better glass hosts that will dissolve higher concentrations of Er³⁺ ions without causing concentration quenching, and at the same time should exhibit a broader FWHM than Al/P silica and ZBLAN. In 1997, Mori and co-workers¹² and Yamada and co-workers¹³ reported the results from an Er³⁺-doped TeO₂ fiber with flat gain over 70 nm covering the range between 1530 and 1600 nm. The device was pumped at 1480 nm and the gain was larger than 20 dB.

Before the Er³⁺-doped TeO₂ amplifiers were invented, these glasses have been known to have a good glass-forming tendency with much better resistance to crystallization and susceptibility to moisture than ZBLAN. The glass has a higher phonon energy (780 cm⁻¹) and refractive index (>1.9) than ZBLAN.^{14–16} The solubility of RE ions in these

glasses is also known to be larger than 5000 ppm.^{9–11} In this paper, we have designed a series of ternary tellurite glasses based on TeO₄, ZnO, and Na₂O oxides as hosts for Er³⁺ ions, and analyzed the structural origin of the emission line-broadening in Er-doped TeO₂ glasses. The spectroscopic properties of tellurite glasses are also compared with a modified silicate and a fluorozirconate glass, called ZBLAN. The structural analysis has been carried out by using Raman and UV-visible spectroscopy for analyzing the structural units and Urbach tail, respectively, of the TeO₂ glasses as a function of the composition. The room-temperature emission spectra in tellurite, ZBLAN, and silicate glasses have been analyzed for their spectral components, which enabled us to determine the spectral width of Stark sublevels and site-to-site variation in each host. A structural model for broadening is also presented. The effect of OH⁻ ions on concentration quenching and the dependence of spectral broadening on Er₂O₃ concentration is also explained on the basis of the structural model discussed herein.

II. EXPERIMENT

The composition of Er³⁺-doped tellurite glass was chosen after a systematic search for stable glass compositions. Multicomponent tellurite glasses are known to be more stable than pure TeO₂ glasses,^{14–16} the latter requires an extreme quenching rate to form. The compositions chosen in this investigation fall in the following composition range: (100 - x - y) mol % TeO₂, x mol %, ZnO, and y mol % Na₂O (see Table I below). The glasses were prepared from 99.99% pure powders of Na₂CO₃, ZnO, Er₂O₃, and TeO₂. Before melting the powders in a gold crucible, the molar masses were calculated, weighted, and mixed thoroughly, using a mortar and pestle. The mixed oxides were melted in a gold crucible at 750 °C in a stream of dry air. At the melting temperature, the oxide melt was homogenized for 30 min and then quenched into a preheated brass mold to form glass. The quenched glass samples were annealed for several hours at 260 °C in a muffle furnace, and then allowed to cool slowly inside the furnace by turning the power supply off. The glass samples were doped with Er₂O₃ in the composition range 500–50 000 ppm. Samples of OH⁻ ion doped glasses were also prepared for spectroscopic analysis. In order to carry out a reliable measurement of emission and absorption spectra, glass samples were polished carefully using a 1- μ m diamond paste.

The analysis of Er³⁺ and OH⁻ ion absorption was carried out using a Perkin-Elmer Lambda-19 UV-visible-NIR and a Fourier transform infrared spectrophotometers, respectively.

The absorption peak for OH^- ion was normalized with respect to the thickness of the glass. Emission in bulk glass was measured using a Ti-sapphire laser to pump at 980 nm. The emission spectra were recorded by scanning spectrometer (Macam Photometrics) equipped with an In-Ga-As detector. The resolution was 1 nm. The 980-nm excitation wavelength was also used to measure the lifetimes of the upper ($^4I_{11/2}$) and the lasing ($^4I_{13/2}$) levels in Er^{3+} -doped glass samples. A mechanical chopper was used to modulate the pump, and fluorescence decay curves were recorded by a digital storage adaptor. The lifetimes were calculated by fitting a single exponential function to the measured data. The structure of glass was analyzed using a Raman spectrometer in the 50–900- cm^{-1} wave-number range in 90° geometry using the Ar^+ -ion laser (514.5 nm) as excitation source. The spectra were observed at an angle of 90° to the propagation direction of the pump beam. The emission spectra of Er^{3+} -doped tellurite and other host glasses used for comparative purposes reported in this paper were analyzed using a peak fit analysis software (SPSS Science). The analyzed Voigtian shapes are described below; for each fitting the value of r^2 was maximized to reduce the standard error. The spectral analysis was carried out in wavelength domain instead of frequency for clarity and convenience. Since the spectral range is so narrow, 200 nm, the error due to conversion is negligible. A Voigtian shape defines both the homogeneous (Gaussian) and the inhomogeneous (Lorentzian) parts. Examples of the Voigtian amplitude are given below, and in some cases, the magnitude of the fitted amplitudes and widths are also given. The thermal characterization of each glass was carried out using a differential scanning calorimeter (DSC-7, Perkin Elmer), in which small fragments (<20 mg) of each glass were heated isochronally at a rate of 10 K min^{-1} to determine the glass transition, crystallization, and peak crystallization temperatures.

III. RESULTS

A. Analysis of vibrational spectroscopic data

Figure 1(a) shows the absorption spectra of OH^- ions in the RR2 glass composition. The OH^- absorption band in RR2 is broader, with a FWHM $\sim 900 \text{ cm}^{-1}$, when compared with fluoride (FWHM 410 cm^{-1}) and silica (FWHM 130 cm^{-1}) glasses. The fundamental OH^- band in TeO_2 glass peaks approximately at 2980 cm^{-1} ($3.356 \mu\text{m}$). The Voigtian components of high-OH peak between 2250 and 3750 cm^{-1} are fitted shown in Fig. 1(b). Each spectral component appears to be at least as broad as observed in the silicate and fluoride glasses. By comparison the fundamental absorption peaks in SiO_2 and fluorozirconate glasses are at $2.72 \mu\text{m}$ and $2.87 \mu\text{m}$, respectively.¹⁷ The broadening of OH^- band in TeO_2 -based glass appears to have a relationship with the glass structure, as, for instance, has been shown for a Na_2O -modified silicate glass, in which the broadening of OH^- fundamental is associated with the presence of non-bridging oxygen. The nonbridging oxygen sites, according to Adams,¹⁸ contribute more to the hydrogen bonding in silica, which is associated with the OH^- absorption.

The structure of TeO_2 glass, described above, was analyzed by Raman spectroscopic technique, and the vibrational

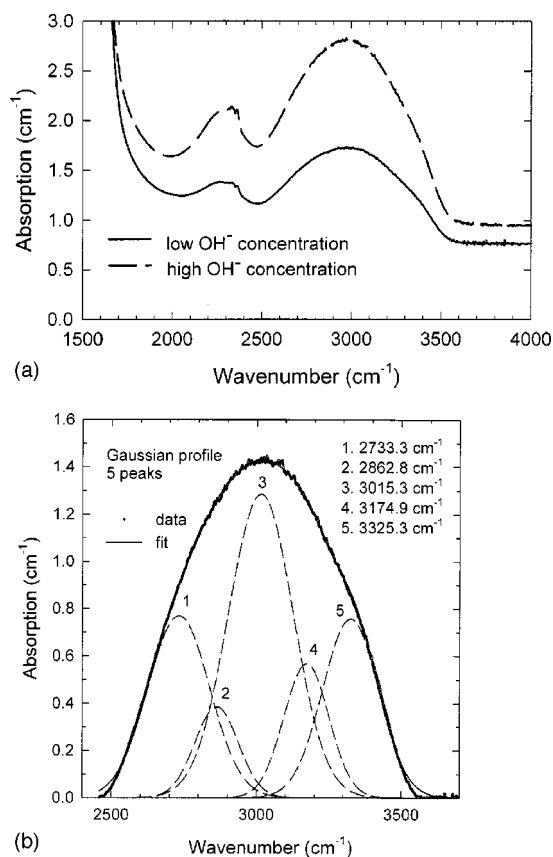


FIG. 1. A comparison of OH^- absorption bands in high and low OH^- ion containing RR2 tellurite glasses. The FWHM in high OH^- RR2 glass is 900 cm^{-1} approximately. (b) A deconvoluted Gaussian amplitude peaks fitted to the broad OH^- absorption band in high OH^- containing RR2 glass.

spectra for all compositions are compared in Fig. 2. In this figure, the symmetric vibrational modes in TeO_2 glasses have been analyzed and assigned. These assignments are based on the data reported in the literature^{16,19–22} for other types of TeO_2 glasses containing modifying oxides, and $\alpha\text{-TeO}_2$ crystals. The assigned vibrations for $\alpha\text{-TeO}_2$ crystals are compared with those determined in glasses, and their relative intensities are compared in Table I. The relative intensities were derived from the peak fit program, which enabled deconvolution of Raman peaks and yielded the relative magnitude of amplitude of each peak. The assigned vibrational modes for peaks in $\alpha\text{-TeO}_2$ and glass compositions are compared in Table II.^{16,19–22}

The analysis of Raman peaks points out that the vibrational modes and their intensities depend on the compositions of divalent and monovalent modifying ions. Since the Raman vibrations are sensitive to the polarizability of the network modifying ions, the larger and more polarizable ions contribute more to intensify the high-energy peaks than the monovalent ions. The high-energy Raman peaks (E and D) are due to the stretching mode contributions not only from TeO_4 trigonal bipyramid (tbp) structural units, but also from $\text{TeO}_{3+\delta}$ polyhedra and TeO_3 trigonal pyramid (tp) units in the environment of nonbridging oxygen.^{20,22} Peak C is assigned to a convolution of antisymmetric vibration modes, arising from the stretching of two dissimilar Te-O bond lengths. Sekiya and co-workers²² proposed that this mode

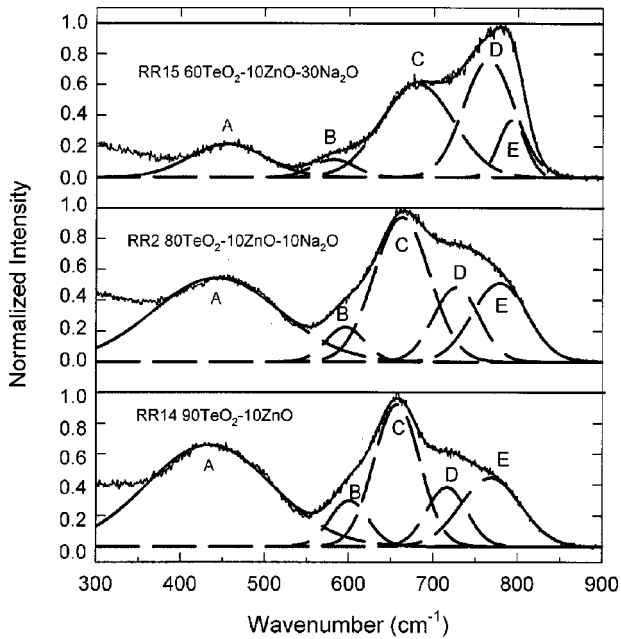


FIG. 2. Relative intensities of Raman peaks in *RR2*, *RR14*, and *RR15* compositions. Excitation wavelength is Ar^+ laser at 514 nm. The curves with broken lines are deconvoluted peaks, *A*, *B*, *C*, *D*, and *E*, which correspond to 450, 611, 659, 716, and 773 cm^{-1} , respectively, in $\alpha\text{-TeO}_2$ (Refs. 18–22).

determines the connectivity between TeO_4 , $\text{TeO}_{3+\delta}$ and TeO_3 structures. According to Komatsu and co-workers,¹⁹ and Himei and co-workers,²¹ two *tbp* structures can connect with each other with an equatorial oxygen. In the same way, two *tp* (TeO_3) and two $\text{TeO}_{3+\delta}$ polyhedra can be connected with each other via an equatorial oxygen. Other combinations of $\text{TeO}_{3+\delta}$ and TeO_4 connectivities are also possible, resulting in a range of antisymmetric vibrations. The antisymmetric vibrations of equatorial oxygens arise due to the presence of the lone-pair electrons (LPE), which leads to the formation of short and long equatorial Te-O bonds,^{17,20} the chemical nature and structure of such bonds are discussed below.

The Raman peaks at lower wave number *A* and *B* are due to the bending (wing mode) and stretching modes of the network as described in Table II. Therefore, the presence of

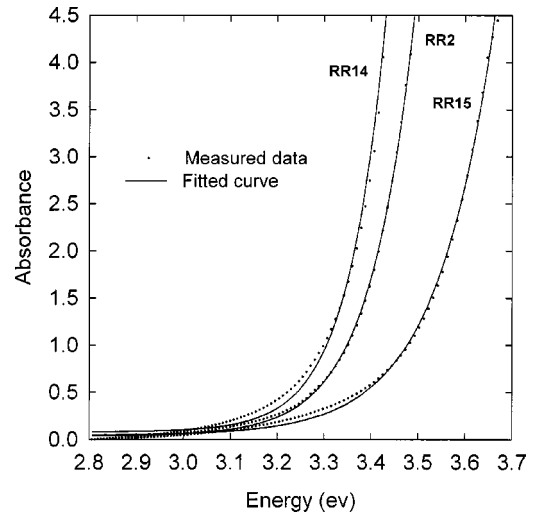


FIG. 3. The measured and fitted electronic absorption edges in *RR2*, *RR14*, and *RR15* tellurite glasses. The derived values of E_0 from fitted Eq. (3) are 5.44, 5.08, and 6.25 eV, respectively.

A and *B* peaks define the network connectivity of TeO_2 glasses.^{19,20,22} On the basis of Raman spectroscopic analysis presented in this paper, which is consistent with the published results,^{14,19–22} it can be concluded that a network modified tellurium oxide glass, for example *RR2* used for doping erbium ions, has more than one type of structural units, namely, TeO_4 , $\text{TeO}_{3+\delta}$, and TeO_3 structures. The extent of deviation between the two oxygen bond distances is strongly dependent on the nature of the modifying oxides.²² Each of these structural units, which depend on the concentrations of modifying oxides,^{20,22} has a unique ligand field and these will vary depending on the value of δ . From the literature,²² it is apparent that the Te-O bond distances are also dependent on the concentration of modifying ions.

B. UV-visible spectroscopy of TeO_2 glass

The UV absorption in samples of *RR2*, *RR14*, and *RR15* glasses were measured by a lamda-19 UV-visible spectrophotometer. The measured Urbach tail for each glass is compared in Fig. 3. The position of tail changes with the composition of the glass, indicating that as the ratio of Te^{4+} to

TABLE II. Vibrational mode assignments for Raman peaks and their comparison with $\alpha\text{-TeO}_2$ structure (Refs. 19–22).

Assigned vibrational modes in TeO_2 glass	$\alpha\text{-TeO}_2$, ν_R (cm^{-1})	Glass ν_R (cm^{-1})		
		<i>RR2</i>	<i>RR14</i>	<i>RR15</i>
Stretching vibrations of Te-O in $\text{TeO}_{3+\delta}$ and TeO_3	773	778	768	793
Vibrations of TeO_4 <i>tbp</i> 's, Te-O_{nbo} in $\text{TeO}_{3+\delta}$ and Te=O_{nbo} in TeO_3	716	730	717	765
Coupled symmetric vibrations along Te-O-Te axes in $\text{TeO}_{3+\delta}/\text{TeO}_4$, $\text{TeO}_4/\text{TeO}_3$ pairs and similar combinations	659	664	657	681
Vibration of continuous $\text{TeO}_3/\text{TeO}_4$ networks	611	591	601	582
Symmetric and bending vibrations of Te-O-Te linkages at corner sharing sites	450	440	421	450

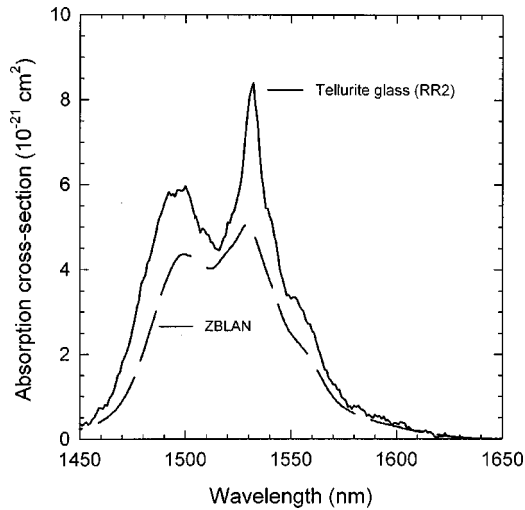


FIG. 4. Comparison of measured absorption cross sections of RR2 and ZBLAN glasses for ${}^4I_{15/2} \rightarrow {}^4I_{13/2}$ transition.

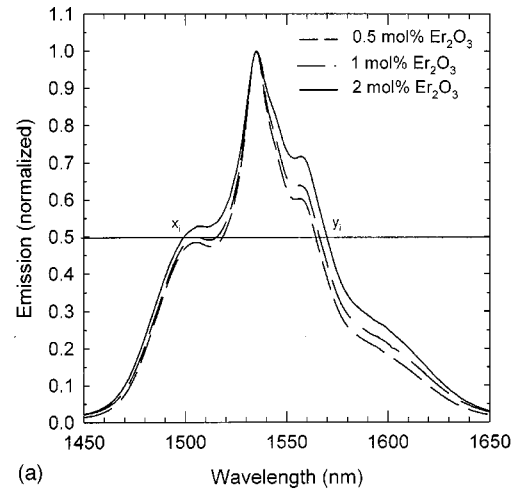
modifying ions ($M^{n+} = \text{Na}^+, \text{Zn}^{2+}$) increases, the position of tail shifts to longer wavelength. The measured electronic edges fit UV energy-gap equation (3) satisfactorily and yields the value of E_0 (eV), which are compared in Table I. For RR15, the Te^{4+}/M^{n+} ratio is 2:1, and the corresponding value of E_0 is 6.25 eV, which decreases to 5.08 eV in RR14 composition having $\text{Te}^{4+}:M^{n+}$ ratio equals to 9:1,

$$\alpha_{\text{uv}} = \alpha_0 \exp\left[-\frac{A(E-E_0)}{\kappa \cdot T}\right] = \alpha_0 \exp[-a(E-E_0)]. \quad (3)$$

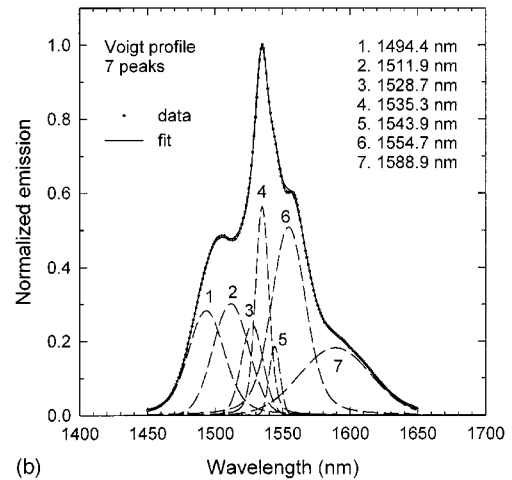
Using the UV-visible–near IR spectrophotometer, the absorption cross sections at 1480 nm in Er^{3+} -ion doped glasses were also measured, and an example is shown in Fig. 4. Evidently, TeO_2 glasses have a much larger cross section than ZBLAN and Al/P silica glasses. A similar trend was also observed for the absorption at 980 nm wavelength.

C. Er^{3+} emission line-shape analysis at room temperature

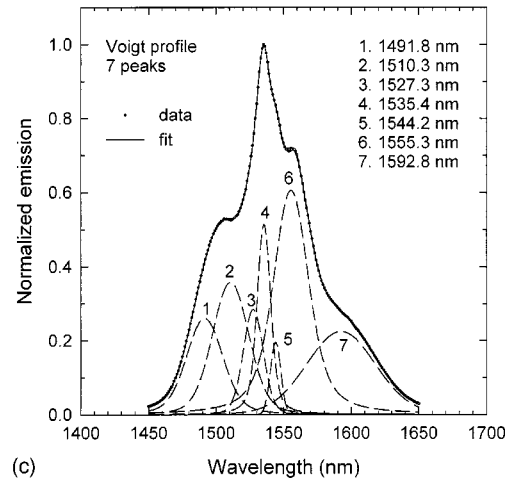
In order to study the effect of Er_2O_3 concentration on ${}^4I_{13/2} \rightarrow {}^4I_{15/2}$ transition and lifetime of the lasing level, RR2 glass was doped with various amounts of Er_2O_3 . Fig. 5(a) shows the fluorescence spectra at different Er^{3+} -ion concentrations; the fitted spectral components for 0.5 and 2 mol % Er_2O_3 are shown in Figs. 5(b) and 5(c), respectively. It illustrates that the higher the concentration of Er_2O_3 doped in the glasses, the broader its emission, while the peak position remains unchanged. Because of the differences in the shape of the emission spectrum in different hosts, FWHM is used as a semiquantitative indication of increase in the bandwidth. Figure 6 compares the FWHM and the wavelength at half maximum fluorescence intensity (HFMI) at different Er^{3+} concentration. The parameter HFMI, plotted in Fig. 6, is defined as the blue (x_i) and red (y_i) wavelengths at FWHM. The relationships plotted as a function of Er_2O_3 concentration in a RR2 glass shows that the FWHM increases gently up to 11 000 ppm, whereas the points x_i and y_i virtually remain unchanged. Above 11 000 ppm concentration, there is a rapid increase in FWHM and in the values of x_i and y_i . Above 20 000 ppm, there is no significant change in the



(a)



(b)



(c)

FIG. 5. (a) Comparison of emission cross sections as a function of Er^{3+} ion concentrations in RR2 tellurite glasses for a ${}^4I_{13/2} \rightarrow {}^4I_{15/2}$ transition. (b) Voigtian spectral components of the overall emission peak for a RR2 glass with 0.5 mol % Er_2O_3 . The widths (w) and amplitudes (a) of 7 Voigtian peaks are (i) 1494.4 nm, (w) 31.57 nm, (a) 0.2935; (ii) 1535.3 nm, (w) 10.35 nm, (a) 0.4906; (iii) 1554.7 nm, (w) 29.14 nm, (a) 0.5198; (iv) 1511.9 nm, (w) 28.73 nm, (a) 0.2889; (v) 1528.7 nm, (w) 18.13 nm, (a) 0.3714; (vi) 1543.9 nm, (w) 9.06 nm, (a) 0.2101; (vii) 1588.9 nm, (w) 50.85 nm, (a) 0.1814. (c) Voigtian spectral components of the overall emission peak for a RR2 glass with 2.0 mol % Er_2O_3 .

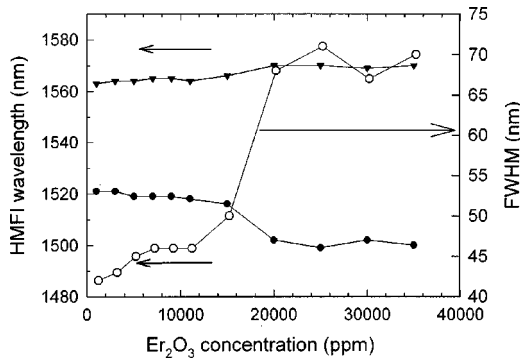


FIG. 6. The dependence of FWHM and HMF on Er^{3+} concentration in RR2 glasses.

shape of the spectrum as function of erbium concentration in the glass. The relationships in Fig. 6 also help in explaining the dependence of the $^4I_{13/2}$ lifetimes on Er^{3+} and OH^- ion concentrations described in Fig. 12.

Figures 7(a), 7(b), and 5(b) compare the normalized emission spectra of Er^{3+} ions doped in three different glass hosts with their fitted spectral components, namely, a modified

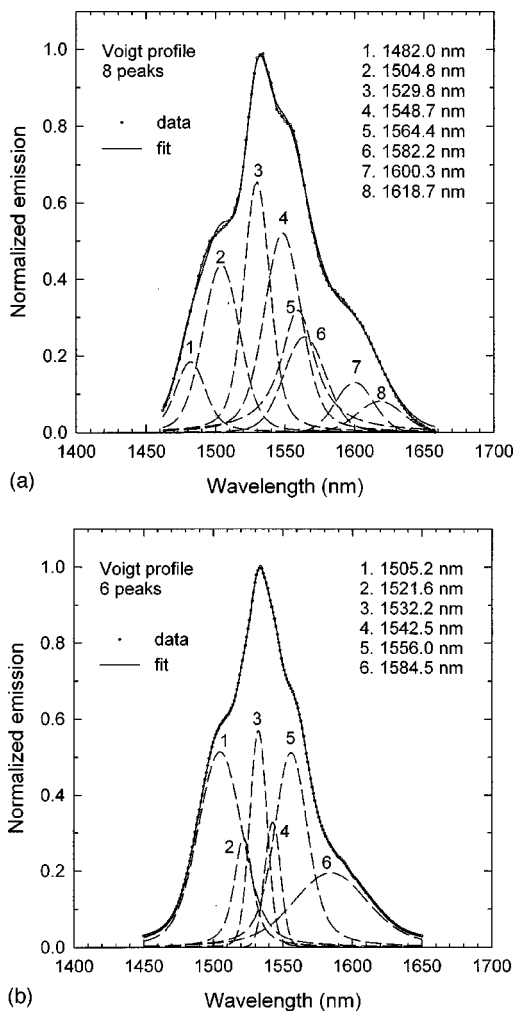


FIG. 7. (a) The emission line for a modified silicate glass (see Tables III and IV) and its eight Voigtian spectral components. (b) The emission line for a ZBLAN glass (see Tables III and IV) and its six Voigtian spectral components.

silicate, fluoride (ZBLAN), and a ternary tellurite glass, respectively. The compositions of these glasses are given in Table III. The concentration of Er^{3+} ions in each host was 1 mol %. The values of emission peak (λ_p nm), FWHM (nm), and emission cross section of Er^{3+} -doped glasses are also compared in this table, from which it is evident that the TeO_2 glasses studied in the present investigation have the largest value of emission cross section ($8.5 \times 10^{-21} \text{ cm}^2$). Unlike the modified silicate and ZBLAN glass hosts studied in this investigation, the spectral broadening in RR2 tellurite glass is much larger with the values of FWHM ranging between 50 and 77 nm, compared to 65 nm in ZBLAN, 44 nm in Al/P silica, and 8 nm in the silicate glass. The main reason for the broadening of emission line shape in tellurite glass is the local ligand field environment of the dopant ions.

The dependence of the emission line broadening of Er^{3+} on the composition of the glass is described below, in which the overall line shape at room temperature has been deconvolved to identify the spectral components, see Figs. 5(b), 5(c), 8(a), and 8(b) for ternary and binary TeO_2 glasses, and Figs. 7(a) and 7(b) for modified silicate and ZBLAN glasses, respectively. Figures 9(a), 9(b), and 9(c) are the examples of the absorption line broadening in two binary tellurite and modified silicate glasses, respectively. The analyzed absorption data for other compositions are summarized in Table IV. On the basis of the peak fit analysis for emission and absorption curves at room temperature, the overall extent of Stark level and sublevel splitting can be determined. In Table IV below, from the peak-fit analysis, the values of the sum of the energy differences between the $^4I_{13/2}$ and $^4I_{15/2}$ levels, $\Delta E_{\text{total}} (\text{cm}^{-1})$ can be found, and compared with the values for ΔE_1 , which is for the ground-state absorption. The difference ($\Delta E_{\text{total}} - \Delta E_1$) is the value of the extent of the Stark splitting of the ground state, $^4I_{15/2}$. The analysis unambiguously demonstrates that the ground state encounters a greater degree of Stark splitting than the $^4I_{13/2}$ level, which is consistent with the earlier findings in the Er-doped silicate glasses.²³ The table also shows that the number of component peaks in a binary tellurite glass is higher than in a ternary glass, thereby proving that as the molar concentrations of modifying oxides increase, the TeO_4 (Raman peak C) to $\text{TeO}_{3+\delta}$ (peaks D and C) and $\text{TeO}_{3+\delta}$ (peaks D and C) to TeO_3 (peak E) structural transformation increase. The presence of larger number of TeO_3 units in RR15, as evidenced in the Raman spectra, Fig. 2, confirms that the continuity of the glass network is substantially decreased, leading to a lesser variation in the environment of Er^{3+} ions from one site to other. As a result, in ternary glasses, there are only seven spectral components [see Figs. 5(b) and 5(c)] compared to 10 in a binary TeO_2 -ZnO glass, see Fig. 8(a). There is also a strong evidence from the spectral analysis of the ternary glasses in Figs. 5(a) and 5(b) that with increasing dopant concentrations the Stark sublevel splitting increases, thereby indicating that the Er^{3+} ions occupy new sites at higher concentrations, which leads to a further line-shape modification.

In Table IV, we have also compared the room-temperature spectral components for three other types of glasses besides binary and ternary tellurite compositions, e.g., a modified silicate and a ZBLAN glass. From the comparison of ΔE_{total} and ΔE_1 values, we find that the ZBLAN glass has the smallest value of ΔE_{total} and ΔE_1 with only six

TABLE III. A comparison of emission cross-section ($\sigma \times 10^{-21} \text{ cm}^2$), metastable lifetime of ${}^4I_{13/2}$ level and FWHM (nm) in tellurite (RR2), modified silicate, and ZBLAN glasses.

Glass composition (mol %)	σ (10^{-21} cm^2)	τ (ms)	FWHM, $\Delta\lambda$ (nm)	$\sigma\tau$	$\sigma\Delta\lambda$ ($\text{cm}^2 \text{ nm}$)
80 TeO ₂ , 9.5 ZnO, 9.5 Na ₂ O, 1 Er ₂ O ₃ (RR2)	8.5	7.5	76 ^a	64 ^a	645
61 SiO ₂ , 11 Na ₂ O, 3 Al ₂ O ₃ , 12 LaF ₃ 12 PbF ₂ 1 ErF ₃ (Modified silicate 193)	7.5	11.0	53	82	398
52 ZrF ₄ , 20 BaF ₂ , 3 LaF ₃ , 4 AlF ₃ , 20 NaF and 1 ErF ₃ (ZBLAN)	5.1	9.5	65	49	331

^a1 mol % Er₂O₃, FWHM for 2 mol % Er₂O₃ is 90 nm in RR2 compositions.

spectral components. By comparison, the modified silicate has eight spectral components for both absorption and emission. At room temperature, the ${}^4I_{13/2}$ Stark level and its sub-components in ZBLAN and TeO₂ glasses have high population density fraction (>0.5), which is determined from the $\exp(-\Delta E_1/kT)$ term. On the other hand, the same level in a modified silicate is less populated due to a larger Stark splitting. The Stark splitting increases with increasing host glass covalency, which is consistent with the comparison of ΔE_1 and ΔE_{ground} values in three different glass hosts discussed in

this work. The bond covalency decreases in the following order: silicate $>$ TeO₂ $>$ ZBLAN. Based on the absorption and emission data for a binary tellurite glass (69 mol % TeO₂, 30 mol % ZnO, 1 mol % Er₂O₃) the transitions between the Stark sub-components are shown in Fig. 10, and the corresponding data for the spread of energy sublevels are also shown in this figure. Due to the lack of low-temperature photoluminescence data, it is not possible to determine precisely the energy sublevels.

The peak-fit analysis of room-temperature emission spectra shows that the individual Stark sublevels have both homogeneous and inhomogeneous broadening. Homogeneous broadening is described by Eq. (1), whereas the inhomogeneous width of each Stark sublevel is due to site-to-site variation and depends on the composition of the glass host. As an example, the amplitude and width of each Stark sublevel is given in Figs. 5(b) and 10. Another important feature of the Stark component analysis is that the short-wavelength (i.e., the bottom sublevels) and the long-wavelength (top sublevels) peaks are much broader than those in the central wavelength regions of both the emission and absorption spectra. This feature appears more dominant in the tellurite glasses than either a silicate or a ZBLAN glass. The comparison of emission line shape and Stark sublevels points out that in fluoride glass hosts, Er³⁺ ions appear to have a much less diversified range of environment due to its ionic character compared to those observed in the covalent TeO₂ and modified silicate glasses. The emission cross section in TeO₂ glasses is higher than ZBLAN and silicates due to their higher refractive index and a larger variation in the Er³⁺ sites. The effect of host glass electric dipole on the electrostatic field and spin-orbit interactions is not distinguishable quantitatively from our present result. However, for glasses with larger atoms (i.e., high Z), the spin-orbit interaction may dominate more than where the host atoms have low Z values. This may be also an important distinction between the Er-doped silicate, fluorozirconate, and tellurium oxide glasses.

For a broadband amplifier, the product, emission cross section (σ_{ab}) times FWHM (λ_{FWHM}) should be large, and the results for RR2, modified silicate, and fluorozirconate glasses are compared in Table III, from which it is clear that the product $\sigma\Delta\lambda$ has the largest value for TeO₂ glasses.

D. Lasing level lifetimes

The decay rate from the ${}^4I_{13/2}$ lasing level in RR2 glass was found to be single exponential in all samples, regardless of Er³⁺-ion concentration. We have shown that the tellurite

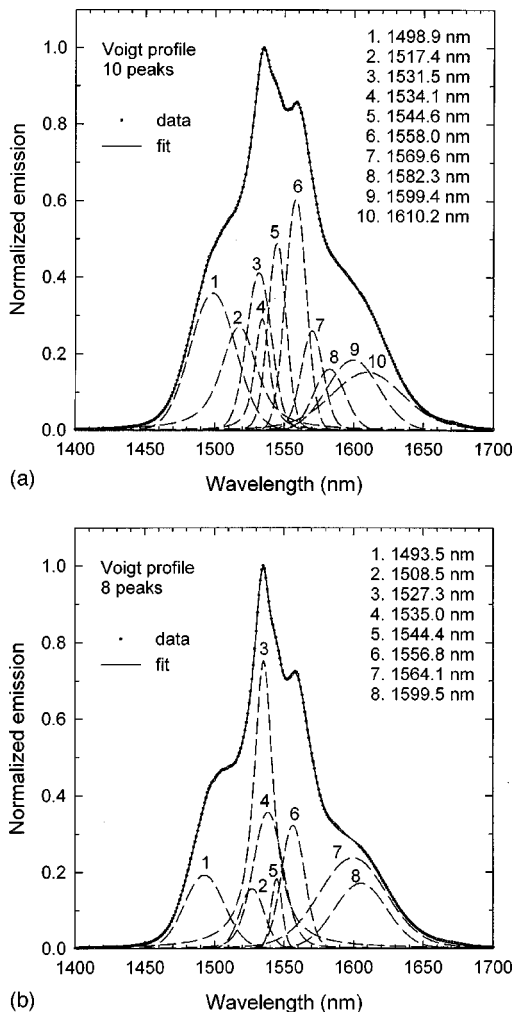


FIG. 8. The fitted Voigtian peaks for two binary tellurite glasses. (a) 70 mol % TeO₂, 29 mol % ZnO, 1 mol % Er₂O₃; (b) 90 mol % TeO₂, 9.5 mol % ZnO, 0.5 mol % Er₂O₃.

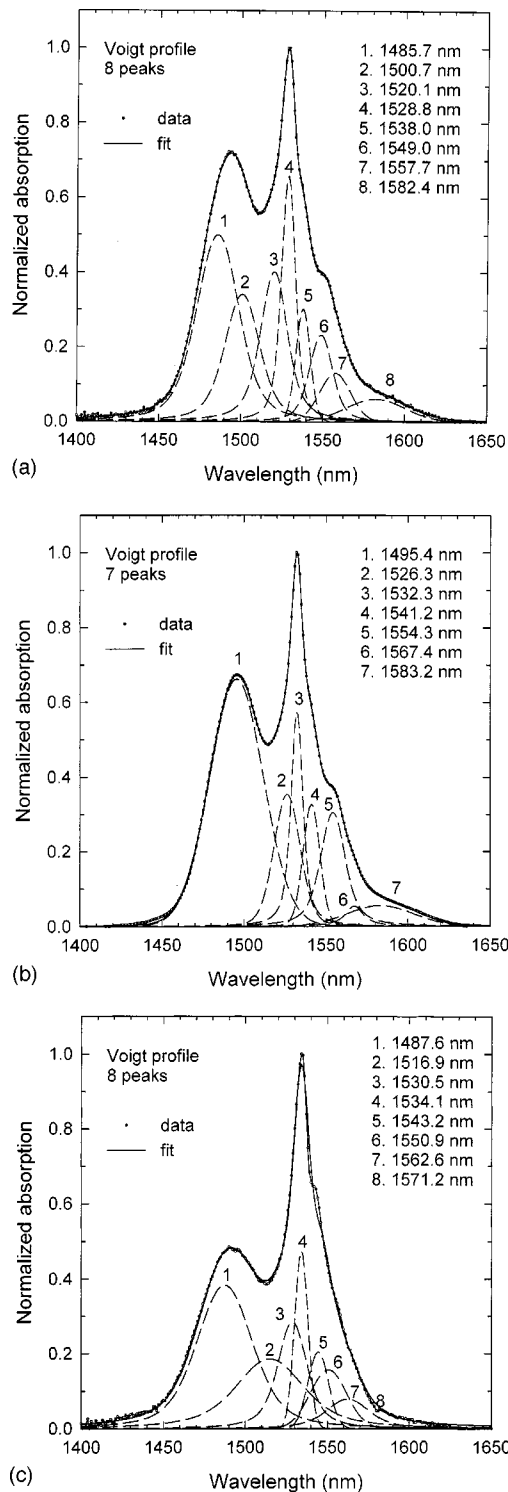


FIG. 9. The fitted Voigtian peaks for the ground-state absorption in two binary tellurite and modified silicate (a) 90 mol % TeO_2 , 9.5 mol % ZnO , 0.5 mol % Er_2O_3 ; (b) 90 mol % TeO_2 , 9.5 mol % Na_2O , 0.5 mol % Er_2O_3 . (c) A modified silicate, see Tables III and IV for composition.

glasses have multiple dopant sites for Er^{3+} ions, and that the $^4I_{13/2}$ emission exhibits a considerable inhomogeneous broadening due to a significant variation between the dopant sites. Therefore, the single exponential decay character of fluorescence decay indicates the presence of fast energy transfer among Er^{3+} ions, which takes place on time scales

much shorter than the decay lifetime, shown in Fig. 11. The goodness of fitted single-exponential equation confirms that the contributions from $2/e$ and $3/e$ folding times are virtually absent. More detailed data analysis confirms that there is an absence of Er-ion clustering even at high doping levels (up to 12 000 ppm), as can be seen in Fig. 12 in which the lifetime changes with Er_2O_3 concentrations from 500 to 45 000 ppm in the RR2 glass with two different OH^- concentrations. The corresponding OH^- -ion absorption spectra for the lifetime versus Er_2O_3 curves shown in Fig. 12 are compared in Fig. 1. These samples were made by melting the RR2 composition at the same temperature for a fixed duration of time, but with two different concentrations of OH^- containing air (high and low OH^-). The low- OH^- concentration samples were melted in dry air, while the high- OH^- samples were prepared in the laboratory air atmosphere. The lifetime versus Er-ion concentration curves in Fig. 12 peak and then drop gently, indicating that the lifetime of the lasing level increases with erbium ion concentration in the OH^- -containing glass. The observed trend in this figure is also consistent with the corresponding change in the value of FWHM plotted as a function of concentration in Fig. 6. At concentrations of erbium ions less than 10 000 ppm, the sharp increase in the lifetime of the $^4I_{13/2}$ level confirms that neither the OH^- -activated quenching nor the ion-ion cross relaxation is a dominating factor. Over and above 15 000 ppm, the lifetime drops more gently in low- OH^- glass than in a high- OH^- glass, indicating that the Er-Er ion cross-relaxation process dominates only after 15 000 ppm. The lower values of the measured lifetimes in high- OH^- glass are not unexpected, which is due to an increase in OH^- -ion induced quenching.

For lower OH^- ion concentration, maximum lifetime of ~ 7.6 ms was observed at around 11 000 ppm Er_2O_3 . With the increase in OH^- ion concentration in host glass, the peak shifts to lower concentration of Er^{3+} ions at around 5 000 ppm having lifetime of ~ 4.9 ms. The values of measured lifetimes reported in this work are at least 1.5 times longer than the values (< 4 ms) reported by the investigators in Ref. 12. Devices with large dopant concentrations and short path lengths are possible without the effect of ion-ion cross relaxation and/or OH^- -induced quenching. By implementing either dry oxygen or air atmosphere processing condition, glasses with low OH^- and large $(\sigma\Delta\lambda)$ product can therefore be designed for a broadband amplifier application.

E. Relaxation behavior of Er_2O_3 -doped TeO_2 glasses

As a part of the structural investigation on TeO_2 glasses, thermal relaxation properties were measured using a differential scanning calorimeter. The glass transition (T_g), onset of devitrification (T_x), and the peak crystallization (T_p) temperatures were measured using a differential scanning calorimeter at an isochronal rate of 10 K mm^{-1} . The values of T_g , T_x , and T_p are plotted as a function of Er_2O_3 concentration in ppm in glass. The three characteristic temperatures increase moderately with Er^{3+} -ion concentration and then level off, see Fig. 13. The increase in T_g and T_x is an indication of strong bonding between Er ion and the host glass, which might be dependent on the concentrations of Er^{3+} ions. The broadening of emission line with increasing erbium

TABLE IV. The analyzed Stark subcomponent from the emission and absorption peak fit analysis. Peak fit data for a binary zinc tellurite glass 69 TeO₂ 30 ZnO 1 Er₂O₃. (i) 1498.9 nm, (w) 39.83 nm, (a) 0.391, area 16.59, (ii) 1558.0 nm, (w) 17.42 nm, (a) 0.659, area 12.23, (iii) 1517.5 nm, (w) 29.75 nm, (a) 0.217, area 6.88, (iv) 1531.5 nm, (w) 22.32 nm, (a) 0.446, area 10.6, (v) 1534.1 nm, (w) 11.83 nm, (a) 0.286, area 4.24, (vi) 1544.6 nm, (w) 14.96 nm, (a) 0.503, area 8.02, (vii) 1569.6 nm, (w) 16.90 nm, (a) 0.303, area 5.45, (viii) 1582.3 nm, (w) 21.92 nm, (a) 0.197, area 4.73, (ix) 1599.3 nm, (w) 39.79 nm, (a) 0.179, area 7.61, (x) 1610.2 nm, (w) 56.51 nm, (a) 0.164, area 9.88.

Composition of glass (mol %)	ΔE_{total} (cm ⁻¹)	ΔE_{ground} (cm ⁻¹)	ΔE_1 (cm ⁻¹)	Fitted peaks	Experiment ($-\Delta E_1 / \kappa T$)
69 TeO ₂ 30 ZnO 1 Er ₂ O ₃	472	412	60	10	0.75
90 TeO ₂ 9.5 Na ₂ O 0.5 Er ₂ O ₃	443	371	72	8	0.71
RR2 with 0.5 mol % Er ₂ O ₃	397	278	120	7	0.56
RR2 with 2.0 mol % Er ₂ O ₃	425	303	122	7	0.55
ZBLAN 1.0 mol % ErF ₃	333	267	66	6	0.72
Modified silicate-193, 1 mol % Er ₂ O ₃	570	357	212	8	0.36

ion concentration strongly suggests that the Er³⁺ ions may be occupying sites as the modifying oxides and stabilizing non-bridging oxygen bonds, which is why the thermal relaxation resistance of glass increases nearly by 20 °C with the addition of Er₂O₃ in the glass. The increase in the characteristic temperatures may also be due to a strong bonding of erbium ions with nonbridging oxygen. This may suggest that Er³⁺ ions due to their high coordination number (which varies between 6 and 7) cannot participate in the formation of glass network.^{14,24} The contribution of 6/7-fold erbium to network formation may be further restricted due to less than fivefold coordination of Te in TeO₂ glass.

IV. DISCUSSION

A. Broadening contribution due to the glass-host structural units

The line strength and the shape of a transition between the states $|j_a\rangle$ and $|i_b\rangle$ is dependent on the electric dipole (\mathbf{D}) and magnetic dipole matrix elements $\langle j_a | \mathbf{D} | i_b \rangle$ and $\langle j_a | \mathbf{M} | i_b \rangle$, respectively, both of ($\chi_{(D)}, \chi_{(M)}$) which are proportional to n^2 , where n is the refractive index of the host. The line strength also depends on the spin-orbit and the crystal lattice field effect, also known as the ion-ligand field. The spin-orbit (LS) mixing is also known to become more dominant with increasing value of Z of rare-earth ions.^{2(a)} However, the LS mixing is also host glass dependent. The analysis of host glass structural units, which determines the environment of dopant ions, is essential in understanding the emission line broadening. The origin of spectral broadening of Er³⁺-ion emission in TeO₂ glasses can be explained on the basis of the structural information deduced from Raman and UV-visible spectroscopic techniques. The discussion focuses on the effect of glass host structure (ion-static host/ion-dynamic host) interaction in Er-doped glasses. The following model for TeO₂ glass network helps us in explaining the emission line broadening in Er-doped glasses. The three different types of structural units TeO₄, TeO_{3+ δ} , and TeO₃ in modified tellurium oxide glasses exist, and their relative pro-

portions are dependent on the chemical nature and the concentrations of the network modifiers used. By comparison, the main structural units in modified silicate and ZBLAN glasses are SiO₄⁴⁻ tetrahedron and ZrF₆²⁻ octahedron. These three different types of structural units must therefore determine the ligand field environment (ion-static, ion dynamic field, and ion-ion cross relaxation, which is also dependent on the structure) of the dopant ion and the host glass. In a pure TeO₂ glass, the TeO₄ structure dominates, and the evolution of TeO_{3+ δ} and TeO₃ commences with the addition of the network modifiers, as has been suggested by several authors in the past.¹⁹⁻²² By referring to the previous structural research in the literature,¹⁹⁻²² the following models for structural changes are proposed, which differ from the previous

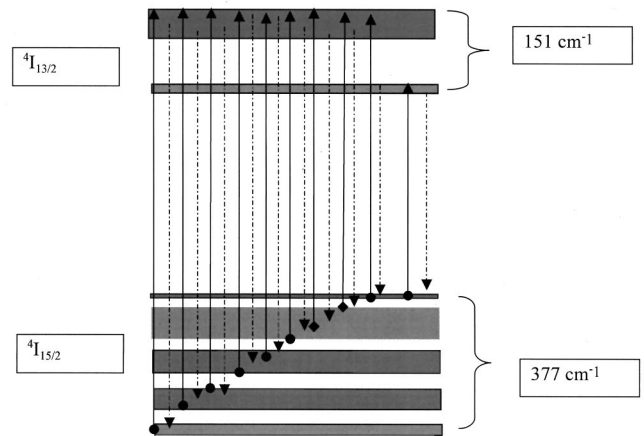


FIG. 10. An illustration of Stark subcomponents in a binary zinc tellurite glass [see Table IV; Figs. 8(a) and 9(a)]. The spectral width of each subcomponent is also given. (i) 1498.9 nm, (w) 39.83 nm, (a) 0.391, (ii) 1558.0 nm, (w) 17.42 nm, (a) 0.659, (iii) 1517.5 nm, (w) 29.75 nm, (a) 0.217, (iv) 1531.5 nm, (w) 22.32 nm, (a) 0.446, (v) 1534.1 nm, (w) 11.83 nm, (a) 0.286, (vi) 1544.6 nm, (w) 14.96 nm, (a) 0.503, (vii) 1569.6 nm, (w) 16.90 nm, (a) 0.303, (viii) 1582.3 nm, (w) 21.92 nm, (a) 0.197, (ix) 1599.3 nm, (w) 39.79 nm, (a) 0.179, (x) 1610.2 nm, (w) 56.51 nm, (a) 0.164.

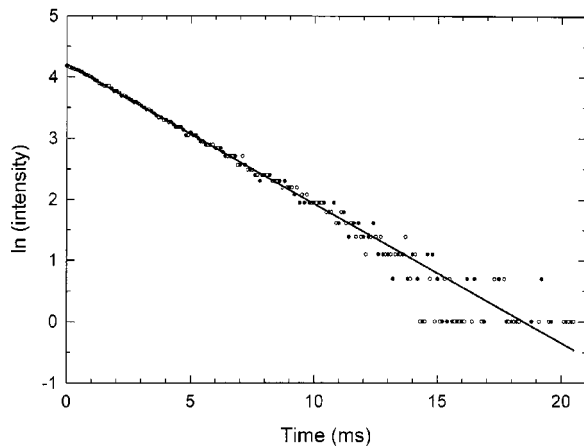


FIG. 11. The measured and fitted single exponential decay rate from ${}^4I_{13/2}$ level to ${}^4I_{15/2}$ in an RR2 glass. Excitation wavelength was 980 nm, and the concentration of Er^{3+} was 0.2 mol %.

structural analysis. The structural model proposed is consistent with the spectroscopic analysis reported in this paper. The approach is based on the understanding of the structural changes observed in the modified silicate and phosphate glasses.

(a) Two fourfold coordinated TeO_4 units combine with a divalent oxide, e.g., ZnO and produce a new unit with Zn^{2+} as a bridging ion between a TeO_3 unit and a TeO_4 unit. The bridging zinc ion (Zn^{2+}) can be considered as a part of a Te_2O_7 (or $\text{TeO}_{3+\delta}$) structure. The zinc ion can also bridge between two TeO_4 tbp's via the bridging oxygen, as shown in Eq. (5). It should be noted that a TeO_3 structure, which is a pyramid with Te at the apex and a double-bonded oxygen, favors an energetically favorable tetrahedron structure by allowing the Te atom at the apex to a new site similar to Te in a tbp structure.

(b) The structural modification to a $\text{TeO}_{3+\delta}$ structure also takes place in the presence of a monovalent sodium ion, as exemplified in Eq. (5), except in the case of sodium ion as a modifier where the zinc ion site is replaced by a bridging oxygen, as shown in Eq. (4). As a result, three nonbridging oxygens are produced, which are distributed over two TeO_4 tbp's. Two such nonbridging oxygen

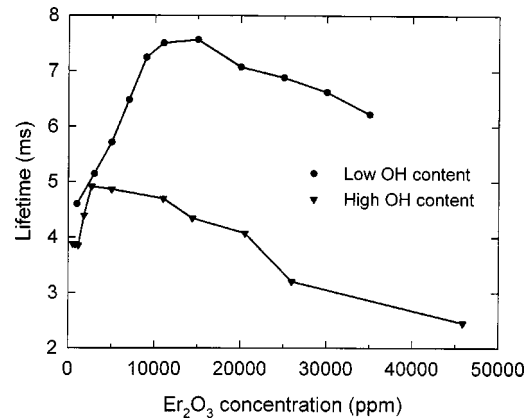
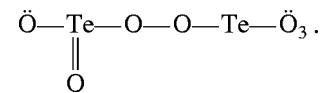


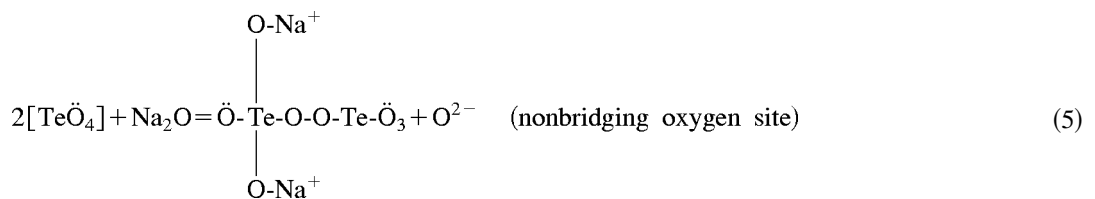
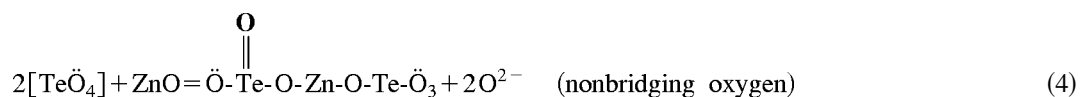
FIG. 12. The dependence of the measured lifetimes of ${}^4I_{13/2}$ level on the concentrations of Er^{3+} at two different OH^- concentrations in RR2 glass.

sites may be similar to those sites, which are shared by, say, Na^+ ions, in Eq. (5); the third one may also become part of the erbium ion environment at a second nonbridging oxygen site.

(c) The third possibility can also be exemplified via Eq. (5), in which a TeO_3 unit can replace a TeO_4 unit by forming a structural unit:



Indeed such combinations of structural units with TeO_3 , $\text{TeO}_{3+\delta}$, and TeO_4 will have a major influence on the ion-host ligand field interaction and contribute to a greater variation between various rare-earth ion-point group sites. By transforming the glass structure from a tbp to a polyhedron $\text{TeO}_{3+\delta}$, which is the most dominant vibrational mode, i.e., peak C, in the Raman spectra, the site for a double-oxygen bonded Te must change to a single-oxygen bonded Te. The presence of multiple structural units is the *first* contributory factor affecting the ion-host interactions both in the static and dynamic fields.



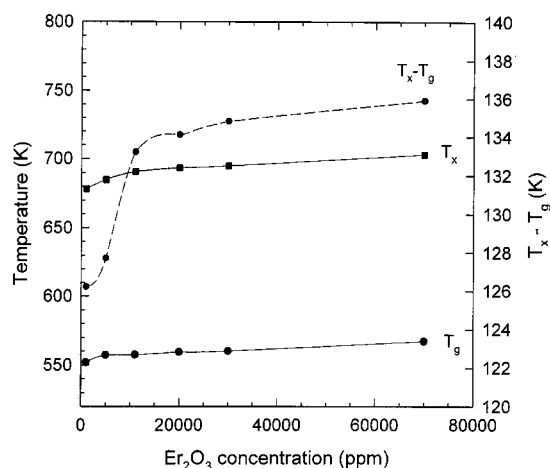


FIG. 13. The dependence of the characteristic glass transition (T_g) and crystallization (T_x) temperatures on Er^{3+} concentrations in RR2 glass.

It has been reported^{18–20} that when modifying oxides, such as BaO, ZnO, and Na₂O, are added in a TeO₂ glass, the TeO₄ network gradually transforms from 4-oxygen coordinated-Te⁴⁺-LPE(Ö) units (tbp) to TeO_{3+δ} polyhedra. The polyhedron structure is the result of a corner-sharing arrangement of TeO₃ (tp) and TeO₄ (tbp) structures, and this is consistent with the model proposed in Eq. (4). Since a TeO₃ and a TeO₄ structure chemically differ, the structural distortion at the oxygen bridging sites shown in Eq. (4) is expected. The evolution of TeO_{3+δ} structure is manifested by changes in the intensities of Raman vibration peak C for antisymmetric structural breathing mode and peak A for the bending mode of the TeO₂ glass structure. As a result of the corner sharing of TeO₄ and TeO₃ units, the bending mode and antisymmetric vibrations of the Te₂O₇ polyhedron structures intensify peak A at 450 cm⁻¹ and peak C at ~660 cm⁻¹ in RR2 glass compared to RR14 and RR15 compositions. The emergence of Te₂O₇ (\equiv TeO_{3+δ}) polyhedron unit, therefore, gives rise to an additional set of weak and strong host ligand Er³⁺ ion interactions. The increased tendency for the formation of TeO_{3+δ} structure shifts the band edge of the TeO₂ glasses to higher energies from 5.08 eV in RR14 (a TeO₂-rich glass) to 5.44 eV in RR2 (see Fig. 3), in which the structure is more modified due to the presence of larger concentrations of Na₂O and ZnO. By comparison, the RR15 composition has the highest concentrations of modifying oxides, Na₂O and ZnO, resulting in the value of band edge at 6.25 eV. The shift in the band-edge energy is also an indication of the change in the cation field strength around the LPE, which may also affect the refractive index of the glass. It is well known that when an alkali (or alkaline-earth) oxide is incorporated in germanate glasses,²⁵ the refractive index increases up to 25 mol % of the modifying oxides, which means that the band edge shifts to lower energy. Because in heavily modified tellurite glasses, the band edge shifts to higher frequency, it can be concluded that the effect of alkali and alkaline-earth oxide additions produces an opposite effect in TeO₂ glasses, which is an important factor in understanding the emission line broadening, as it depends on the value of $\chi (= E_{loc}/E)$. On the basis of the analysis of Raman data and the measured UV-edge results, it can be concluded

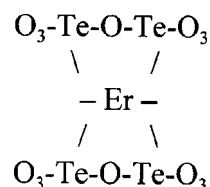


FIG. 14. The schematic diagram of sixfold Erbium coordination via LPE in a TeO₂ glass structure.

that the formation of Te₂O₇ structure with different modifying cations produces additional environments for Er³⁺ ions in TeO₂ glasses, around which the possible bond configurations for LPE increase. The combination of LPE and Te₂O₇ structural units is the *second* contributory in producing a wide variety of ligand-ion environment and field strengths around Er ions. It should be noted that the lone-pair electrons are completely absent in fluoride and silicate, phosphate, and borate glasses.

The modifying cations, as expected, also create nonbridging oxygens in the tellurite glass structures, as they do in the silicate, phosphate, borate, and germanate glasses. In silica glass, the solubility of RE ions is low and extensive ion clustering takes place. The clustering of RE ions is significantly reduced by the addition of Al³⁺ and P⁵⁺ ions, which modify the silica structure and disperse the RE ions in the environment of nonbridging oxygens.^{26–28} Arai and co-workers²⁶ showed that the dispersion of Nd³⁺ ions in Al/P-containing silica is much better than in pure silica; the same glass also exhibits a much better solubility and ion-ion separation between erbium ions. As a result, the 1500 nm emission in Er-doped Al/P is much broader than in pure silica.^{2(a),27,28} A similar effect is seen in the TeO₂ glass due to the addition of modifying oxides. Wells,²⁹ on the basis of the crystal structures of lanthanide sesquioxides, describes higher than six coordination of Er in the Er₂O₃ oxide crystals. Such possibilities may also exist, which cannot be substantiated in this paper without a detailed glass structure, particularly with reference to the sites for RE ions. From the crystal coordination chemistry of sesquioxides, an erbium ion therefore may assume either a sixfold or sevenfold coordination by sharing the LPE, as shown in Fig. 14. Alternatively it may choose to share the nonbridging oxygen sites, as does a sodium ion, shown in Eq. (5). The Er³⁺ ions at such sites will be then surrounded by six or seven TeO₄ units by forming an octahedral-like cage. The possibility of more than one type of coordination for an Er³⁺ ion in a tellurite glass host is the *third* contributory factor.

B. Broadening of OH⁻ absorption peak

The multiplicity of LPE sites and nonbridging oxygens is responsible for the extensive broadening of OH⁻ peak in a TeO₂ glass, which is consistent with the model proposed by Adams.¹⁸ A wide range of structural sites, which are present in a TeO₂ glass, is not available in the SiO₂, fluoride, and germanate glasses. As a result OH⁻ ions disperse and form hydroxyl bonds over range of sites. Arnaudov and co-workers³⁰ proposed the sites in barium-tellurite glasses are due to TeO₃-O⁻·HOTeO₄ units. The authors suggested that “the oxygen atom-electrodonors are strongly polarized and become nonbridging sites.”

In the present investigation, from the spectroscopic observations of Er^{3+} - and OH^- ions, the behavior of hydroxyl ions appears more complex and is described below. The oxide anion in OH^- acts as an oxygen donor to TeO_n structures at the LPE sites at lower concentrations of OH^- (see effect of OH^- on lifetimes of $^4I_{13/2}$ level in Fig. 11). By considering the approach of Arnaudov and co-workers, we can consider that when an LPE site transforms into a nonbridging donated oxygen site (NDOS), by accepting the oxide anion from OH^- , and then forms a bond with the neighboring Er^{3+} ion, there would be a net negative charge deficiency in the environment of Er^{3+} ion. The donation of oxygen will necessitate that the protons (H^+ ion) must move away at least into a second coordination cell of Er^{3+} ion. This would also mean that the new O-H^- bond due to the release of a proton will not be available in the immediate vicinity of Er^{3+} to induce the quenching of luminescence. The modifying ions in the same way donate oxygen to LPE sites to form NDOS and cause a major shift in the position of Urbach tail to short wavelengths (see Table I, E_0 values). It is expected that in the presence of Er^{3+} ions coupled with NDOS, the excess protons will contribute to more nonbridging oxygen sites away from the original LPE sites. These may become evident from the increase in the intensity of peaks *C* and *D* in Raman spectrum of the glass. Once all the LPE sites have transformed into NDOS's, the ion-ion cross relaxation becomes dominant. There is an additional complementary information on the effect of OH^- ions on quenching of Er luminescence. The initial slope of lifetime versus Er_2O_3 concentration is steeper in glasses with higher concentrations of OH^- than glasses with lower OH^- . This difference in the initial slopes between high and low OH^- glasses suggests that there are much fewer LPE sites, which have not transformed to NDOS's in a high-OH glass than in a low-OH glass. It is, therefore, possible to control LPE's and NDOS's by selecting a gaseous atmosphere together with the modifying cations in tellurite glass.

C. Prolonged metastable lifetime

There are two main reasons for a prolonged lifetime of 7.8 ms in 11 000 ppm doped TeO_2 glass structure. The first one is associated with an increased ion-ion separation distance, which may be at least of the order of 0.390 nm (two times the shortest Te-O bond), if not more, which can be estimated by considering the structural model in Fig. 14. The second one is due to the increased $\text{Er}^{3+}/\text{OH}^-$ ion distance. As proposed above, the LPE/NDOS transformation in the TeO_2 glass structure (and hence $\text{Er}^{3+}/\text{NDOS}$ interaction) causes the H^+ protons to move away in the second or higher coordination shells. As a result, on average the Er-OH separation distance is at least going to increase by a factor of 4. With the increasing distance, the probability of impurity-induced quenching is greatly reduced. In the present investi-

gation, we have also measured the lifetimes of $^4I_{13/2}$ level in silicates and fluorozirconate glasses (ZBLAN). In each case the measured total lifetimes vary between 10 and 11 ms. The refractive indices of silicates and ZBLAN glasses range between 1.45 and 1.51, which are significantly lower than the average index of a tellurite glass composition (~ 2.1) discussed above. The radiative rate increases with the square of refractive index of the host, which means that a factor of nearly 2 is required to compare the measured lifetimes of tellurite glasses with those of silicates. The measured lifetimes of $^4I_{13/2}$ level for Er-doped silicates and ZBLAN are approximately 12 ms, which by comparing the measured lifetime and refractive index of an Er-doped tellurim oxide glass refractive index, should be of the order 15–16 ms, thereby indicating that in the silicate and ZBLAN glass hosts due to the structural constraints, the erbium ions are neither uniformly dispersed nor they can be dissolved in higher concentrations compared to a TeO_2 glass. The measured long lifetime at higher concentrations of Er^{3+} ions in the tellurite glasses may not be just due to the nonradiative component, but also due to the structural factors, which we are unable to distinguish in the present investigation.

V. CONCLUSIONS

(a) There are three major structural factors due to the host glass, which contribute to line-shape broadening in Er-doped TeO_2 glasses. The first contribution is due to the presence of three different types of structural units in the TeO_4 structure, which causes the Te-O bond length to change in equatorial and axial directions. As a result, the ion-host field strengths change. The second contribution arises due to a change in the interaction between an LPE and the modifying cations, e.g., Zn^{2+} , Na^+ . The third contribution arises due to more than one type of coordination of Er^{3+} in a tellurium oxide glass. The combination of these factors contribute to the line-shape broadening.

(b) The broad OH^- ion absorption band in TeO_2 glass is due to the multiplicity of sites, where a nonbridging oxygen forms with the TeO_3 , TeO_4 , and Te_2O_7 structures.

(c) The OH^- ions donate oxygens to LPE sites and release protons, which occupy sites away from Er^{3+} -ion sites. The increased Er-OH ion separation distance reduces the probability of OH-induced quenching of the metastable $^4I_{13/2}$ level in Er ions. The release of proton increases the Er-Er ion distance. As a result ion-ion clustering diminishes rapidly. These two factors contribute in prolonging the lifetimes of $^4I_{13/2}$ level to 7.8 ms in 11 000 ppm doped glasses besides the radiative components.

ACKNOWLEDGMENTS

The authors acknowledge the help and guidance given by Professor Rui Almeida and Dr. L. Santos for carrying out the Raman spectroscopic experiments at INESC, Lisbon.

*Corresponding author. Email address: a.jha@leeds.ac.uk

¹S. Sudo, *Optical Fibre Amplifiers—Materials, Devices, and Applications*, 1st ed. (Arctec House, Boston, 1997), pp. 178–181.

²(a) W. J. Miniscalco, in *Optical and Electronic Properties of Rare Earth Ions in Glasses in Rare Earth Doped Fibre Lasers*

and Amplifier, edited by M. J. F. Digonnet (Dekker, New York, 1993), pp. 25–30; (b) *ibid.*, pp. 82–84.

³J. N. Sandoe, P. H. Sarkies, and S. Parke, *J. Phys. D* **5**, 1788 (1972).

⁴E. S. Georges (unpublished).

- ⁵W. J. Miniscalco, J. Lightwave Technol. **LT-9**, 234 (1991).
- ⁶M. Semenkoff, M. Guibert, D. Ronarch, Y. Sorel, and J. F. Kerdiles, J. Non-Cryst. Solids **184**, 240 (1995).
- ⁷T. Whitley, C. A. Miller, R. Wyatt, M. C. Brierly, and D. Szabert, Electron. Lett. **27**, 1785 (1991).
- ⁸M. C. Brierly, C. A. Miller, and P. W. France (unpublished).
- ⁹R. Reisfeld and Y. Eckstein, Solid State Commun. **13**, 741 (1973).
- ¹⁰R. Reisfeld and Y. Eckstein, J. Non-Cryst. Solids **15**, 125 (1974).
- ¹¹R. Reisfeld and Y. Eckstein, J. Non-Cryst. Solids **12**, 357 (1973).
- ¹²A. Mori, Y. Ohishi, and M. Yamada (unpublished).
- ¹³M. Yamada, A. Mori, K. Kolayashi, H. Ono, T. Kanamosi, K. Oikavia, Y. Nishida, and Y. Ohishi, IEEE Photonics Technol. Lett. **10**, 1244 (1998).
- ¹⁴J. E. Stanworth, Nature (London) **169**, 581 (1952).
- ¹⁵G. W. Brady, J. Chem. Phys. **24**, 477 (1956); *ibid.* **27**, 300 (1957).
- ¹⁶W. Vogel, in *Chemistry of Glasses*, 2nd ed., edited by N. Kreidl (The American Ceramic Society, Westerville, OH, 1985), pp. 167–174.
- ¹⁷P. W. France, *Fluoride Glass Optical Fibres* (Blackie, London, 1990), pp. 135–142.
- ¹⁸R. V. Adams, Phys. Chem. Glasses **2**, 50 (1961).
- ¹⁹T. Komatsu, H. G. Kuin, and H. Mohri, J. Mater. Sci. Lett. **15**, 2026 (1991).
- ²⁰J. C. Sabadel, P. Armand, D. Cachan-Herreillat, P. Baldeck, O. Doctot, A. Ibanez, and E. Philippot, J. Solid State Chem. **132**, 911 (1997).
- ²¹Y. Himei, A. Osaka, T. Nanba, and Miura, J. Non-Cryst. Solids **177**, 164 (1994).
- ²²T. Sekiya, N. Mochida, and A. Ohtsuka, J. Non-Cryst. Solids **168**, 106 (1994).
- ²³E. Desurvire and J. R. Simpson, Opt. Lett. **15**, 547 (1990).
- ²⁴J. H. Simmons, C. J. Simmons, R. Ochoa, and A. C. Wright, in *Fluoride Glass Fiber Optics*, 1st ed., edited by G. Lu and I. D. Aggarwal (Academic, New York, 1991), pp. 40 and 41.
- ²⁵A. Paul, *Chemistry of Glasses*, 2nd ed. (Chapman and Hall, London, 1990), p. 104.
- ²⁶K. Arai, H. Namikawa, K. Kumata, and T. Honda, J. Appl. Phys. **59**, 3430 (1986).
- ²⁷A. Nakazawa and Y. Kimnsa, Electron. Lett. **27**, 1065 (1991).
- ²⁸M. Ohashi and K. Shiraki, Electron. Lett. **27**, 2143 (1991).
- ²⁹A. F. Wells, *Structural Inorganic Chemistry* (Clarendon, Oxford, 1962), pp. 464–467.
- ³⁰M. Arnaudov, Y. Dimitriev, V. Dimitrov, and M. Dimitrova-Pankova, Phys. Chem. Glasses **27**, 48 (1986).